Insights into the evolution of the Hindu Kush-Karakoram from modern river detrital geo- and thermochronological studies

Guangsheng Zhuang[1, *], Yani Najman[2, *], Yuntao Tian[3], Andrew Carter[4], Lorenzo Gemignani[5], Jan Wijbrans[5], M. Qasim Jan[6], and M. Asif Khan[7]

[1] Department of Geology and Geophysics, Louisiana State University, Baton Rouge, LA 70803, USA

[2] Lancaster Environment Centre, Lancaster University, LA1 4YQ, Lancaster, UK

[3] School of Earth Sciences and Engineering, Sun Yat-sen University, Guangzhou, 510275 China

[4] Department of Earth and Planetary Sciences, Birkbeck, University of London, London WC1E 7HX, UK

[5] Department of Isotope Geology, Vrije Universiteit, De Boelelaan 1085, 1081 Amsterdam, Netherlands

[6] National Centre of Excellence in Geology, University of Peshawar, Peshawar 25130, Pakistan.

[7] Karakoram International University, Gilgit, Pakistan

[*] gzhuang@lsu.edu, y.najman@lancaster.ac.uk

Abstract:

The evolution of Hindu Kush and Karakoram remains elusive due to the limited knowledge of crustal accretion and exhumation history. Here, we present a synoptic study of detrital zircon U-Pb geochronology and detrital muscovite $^{40}Ar/^{39}Ar$ thermochronology from modern river sediments, and numerical models on $^{40}Ar/^{39}Ar$ dates to characterize this region. Our study supports the presence of 200 Ma zircons in the Hindu Kush, which is interpreted as the result of the amalgamation of the Hindu Kush-South Pamir to the Central Pamir at this time. Detrital zircon U-Pb age peaks of 110–130 Ma, 60–80 Ma peak, and <28–40 Ma seen in the modern river sediments capture phases of crustal growth prior and subsequent to India-Asia collision. Inversion of muscovite $^{40}Ar/^{39}Ar$ dates suggests high erosion rates prior to the India-Asia collision (at ca. 115–128 Ma and 71 Ma) and after collision (35 Ma, 27 Ma, and 8 Ma). The data show considerable variation between different areas. Most strikingly, 8 Ma rapid exhumation is only recorded in the east-central Karakoram, reflecting east-west along-strike variation in exhumation, as previously documented with respect to metamorphic and magmatic episodes, or the proximity of river headwaters to the Karakoram Fault.

1. Introduction

The present-day high topography of the western parts of the Himalaya and Tibetan Plateau (Fig. 1A) represents a manifestation of complex interactions between tectonism, surficial erosional processes, and climate (e.g. Brozović et al., 1997; Maheo et al., 2002; Searle, 2015; Van Der Beek et al., 2009; Wallis et al., 2016). Hence, study of the crustal thickening and exhumation of the region bears on implications for better understanding of these tectonism-erosion-climate interactions.

In constraining the spatial-temporal erosion history of the western Himalaya and Tibetan Plateau, bedrock vertical transect studies, so called "in situ thermochronology" (Braun et al., 2006), demonstrate the utility of densely sampling basement rocks (intervals of 100s meters in vertical scale) along with thermal modeling, which provide extra information on particle trajectories during exhumation towards the surface (e.g. Van Der Beek et al., 2009). Whilst these studies have high spatial resolution, the ability of vertical transect studies is limited in temporal range due to the loss of old rocks at structurally high horizons which have been removed during the earlier stages of orogenesis; such rocks contain critical information about tectonism and erosion beyond the present-day mountain belt (Braun et al., 2006; Clift et al., 2004). Hence, a substantial amount of effort in thermochronology has also been focused on the products of erosion, i.e. the detritus present in fluvial systems and preserved in the receiving basins, which has greatly extended the temporal record of orogenesis (Braun et al., 2006; Reiners and Brandon, 2006).

In the Hindu Kush-Kohistan-Karakoram (Fig. 1B), there is evidence for growth of high topography both prior to (e.g. Robinson 2015) and shortly after (e.g. Carter et al., 2010; Van der Beek 2009) India-Asia collision. Various episodes of crustal thickening and exhumation have been documented from collision until present day (e.g. Cerveny et al., 1989; Dunlap et al., 1998; Foster et al., 1994; Krol et al., 1996a; Wallis et al., 2016), and much work has focused on the Nanga Parbat syntaxis (e.g. Schneider et al., 2001; Zeitler et al 2001). Despite these studies, knowledge of this region remains spatially and temporally incomplete.

To evaluate the regional variations in erosion and to extend the temporal range in order to better understand the long-term evolution of the region, we undertook a detrital study based on muscovite $^{40}Ar/^{39}Ar$ thermochronology on modern river sediments. The closure temperature of muscovite $^{40}Ar/^{39}Ar$ thermochronology (>350 °C) (McDougall and Harrison, 1999), with a geothermal gradient of 25 °C/km, would suggest that muscovite $^{40}Ar/^{39}Ar$ thermochronology can detect crustal exhumation processes originating from depths greater than 10–15 km. We combined detrital muscovite $^{40}Ar/^{39}Ar$ thermochronology with modeling results of erosion, as well as detrital zircon U-Pb analysis, the latter to provide insight to crustal thickening in the region.

2. Geological setting

Our research area is located in the western part of the Himalaya and Tibetan Plateau (Fig. 1A). Here, the India-Asia suture is characterized by the Cretaceous-Paleogene Kohistan Oceanic Island arc (Pudsey et al., 1985; Searle et al., 1987; Tahirkheli et al., 1979; Treloar and Izatt, 1993) which is sandwiched between the Indian and Asian plates. There is thus a double suture zone, with the Main Karakoram Thrust (MKT) or Shyok Suture Zone (SSZ) in the north separating the Kohistan arc from the Asian plate, and the Main Mantle Thrust (MMT) or the Indus Suture Zone (ISZ) in the south, separating the Kohistan arc from the Indian plate (Fig. 1B). Our research area covers the Hindu Kush and Karakoram of the Asian plate, which formed an Andean-style margin prior to India-Asia collision (Hildebrand et al., 2000; Khan et al., 2009; Searle et al., 1987), and the Kohistan island arc (Fig. 1B).

Timing of collisions between the active margin of Asia (Karakoram, Hindu Kush and to the east the Lhasa terrane), India, and the Kohistan arc is debated. Whilst evidence has been provided both that the Kohistan arc collided first with Asia prior to ~85–90 Ma (Faisal et al., 2014; Petterson et al., 1985; Searle et al., 1999; Treloar et al., 1989) or with India at 65 or 50 Ma (Bouilhol et al., 2013; Khan et al., 2009), terminal suturing between India and Asia is considered by a majority of researchers to have taken place by 60–55 Ma (DeCelles et al., 2014; Hu et al., 2016; Najman et al., 2017), although some have argued that it may have continued until circa 35 Ma or 25–20 Ma (Aitchison et al., 2007; Bouilhol et al., 2013; van Hinsbergen et al., 2012).

Both the Hindu Kush and the Karakoram are Gondwana terranes that drifted across the Tethys and collided with Asia during the Mesozoic Cimmerian orogeny (Angiolini et al., 2013; Şengör, 1984). The Hindu Kush is considered to be the western continuation of the Wakhan Block — part of the South Pamir, both comprising an extended crust (Faisal et al., 2014; Zanchi et al., 2000). The Hindu Kush consists of deformed granitoids of Cambrian-Precambrian age, Paleozoic-Mesozoic metasedimentary successions, and Jurassic to mid-Cretaceous granitoids (Zanchi et al., 2000). The Hindu Kush-South Pamir collided with the Central Pamir along the Rushan-Pshart suture zone around the Triassic-Jurassic boundary (Angiolini et al., 2013), as recorded by metamorphic monazites with U-Pb ages of ~200 Ma (Faisal et al., 2014).

To the south the Hindu Kush-South Pamir is separated from the Karakoram by the Wakhan-Tirich boundary zone (Fig. 1B), with these two terranes docking in Early Jurassic times, as recorded by monazite U-Pb ages of ca. 185 Ma (Angiolini et al., 2013;

Faisal et al., 2014; Zanchi and Gaetani, 2011). Following this crustal accretion event, an Andean-style subduction system was established to the south of the Karakoram which was responsible for the development of a continental magmatic arc along the Karakoram, as evidenced by, for example, the intrusion of the Karakoram Batholith at 95–130 Ma (e.g. Debon et al., 1987; Fraser et al., 2001; Heuberger et al., 2007). Late Cretaceous monazites (Faisal et al., 2014) were interpreted to record regional metamorphism associated with the re-establishment of a subduction system farther to the south after the docking of Kohistan arc prior to 85–90 Ma (Fraser et al, 2001; Searle et al., 1999; Treloar et al., 1989).

The Karakoram terrane is broadly divided into three main units (Hildebrand et al., 2000; Searle et al., 1999), the Northern Karakoram Terrain, the Southern Metamorphic Complex, and the intervening batholith (Fig. 1B). The Northern Karakoram Terrain consists of a mostly sedimentary belt which comprises pre-Ordovician crystalline basement covered by an Ordovician to Cretaceous sedimentary succession (e.g. Gaetani and Garzanti, 1991; Zanchi and Gaetani, 2011). The Karakoram Batholith includes pre-India-Asia collision, Andean-type, subduction-related granitoids (e.g. the Hunza Batholith) as described above, and post-collision leucogranites (e.g. the Baltoro Batholith) (Fig 1B). The formation of the Baltoro Plutonic Unit of the Karakoram Batholith, dated between ca. 25 Ma and 13 Ma, represents post-collision crustal thickening culminating in crustal melting (Parrish and Tirrul, 1989; Searle et al., 2010). Localized crustal melting and leucogranite intrusion in the Garam Chashma area of Hindu Kush at 29–22 Ma (Faisal et al., 2014; Hildebrand et al., 1998) is contemporaneous with this event.

Metamorphism of the Southern Karakoram Metamorphic Belt spans from pre India-Asia collision to Late Miocene but the record is spatially varied; metamorphic ages as old as Late Cretaceous are documented in the Hunza region to the west, whilst along strike in the Baltoro region to the east no ages older than Late Oligocene are recorded (Palin et al 2012; Searle et al 2010). Pre India-Asia collision regional metamorphism is interpreted as due to Asia-Kohistan Arc collision. Post India-Asia crustal thickening and regional metamorphism is recorded in the Early Miocene in the Hunza region, and with approximately co-eval crustal melting in the Baltoro region as described above. The most recent phase of regional metamorphism occurred in the Late Miocene in the Baltoro region (Fraser et al 2001).

A disproportionate number of exhumation studies of the NW Himalayan region have focused on the Nanga Parbat syntaxis where >15 km crustal materials were denudated in the past 3 Ma (e.g. Schneider et al., 2001; Zeitler et al 2001) and the Karakoram Fault region (Boutonnet et al., 2012; Dunlap et al., 1998; Foster et al., 1994; Krol et al., 1996a; Mukherjee et al., 2012; Schärer et al., 1990; Wallis et al., 2016). For example, several phases of rapid cooling associated with thrusting and strike-slip motion of the Karakoram Fault were constrained by $^{40}Ar/^{39}Ar$ (hornblende, muscovite, biotite, and K-feldspar) and apatite fission track to be at 17–13 Ma & 8–7 Ma and 7.4–3.3 Ma (Dunlap et al., 1998; Wallis et al., 2016). Contrasting with these young ages of rapid exhumation in the eastern Karakoram, studies including apatite and zircon fission track analysis and K-Ar and Ar-Ar dates (biotite, hornblende, and muscovite) show that Cretaceous/Paleocene-Eocene cooling ages have been reported in the west including western Kohistan, East Hindu Kush, and the South Karakoram Metamorphic Belt (Treloar et al., 1989; Zeitler, 1985).

In the western Himalaya, the tectonostratigraphic zones that were identified in the central and eastern Himalaya, including Lesser, Higher, and Tethyan Himalayan zones, can be correlated to some extent, but they are not continuous with their correlatives to the east due to the lack of clear traces of major faults, like the Main Central Thrust (DiPietro and Pogue, 2004). Additionally, unlike the main arc of the orogen, Neogene leucogranites are absent in the western Himalaya. By contrast, much of the metamorphism and deformation recorded in the western part of the orogen occurred prior to late middle Eocene. For example, zircons from the Malakand Granite of the Swat region give a mean U-Pb age of 47 Ma for the rims and an age range of 254–291 Ma for the cores, reflecting the earliest phase of Himalaya orogeny and the presence of Carboniferous igneous suites in the western Himalaya, respectively (Smith et al., 1994).

3. Methodology

In order to obtain an overview of the geological evolution of the region, detrital muscovite $^{40}Ar/^{39}Ar$ thermochronology and detrital zircon U-Pb geochronology analyses were applied to six modern river sand samples draining the Hindu Kush, Karakoram and Kohistan Island Arc (Figs. 2 and 3; Table 1; Tables S1 and S2). Zircon U-Pb analyses were undertaken to study crustal accretion and muscovite $^{40}Ar/^{39}Ar$ analyses to study exhumation. We apply a multidimensional scaling (MDS) method for analyzing detrital zircon U-Pb data regarding provenance analysis (Fig. 4) and new MATLAB codes to implement the inversion of muscovite $^{40}Ar/^{39}Ar$ dates to erosion rates (Figs. 5 and 6; Table S3).

3.1. Modern river sediment samples

Six modern river sand (MRS) samples were taken from the western Himalaya and Tibetan Plateau (Fig. 1). Sample information including sampling coordinates is provided in Table 1. MRS 3 was taken from the Hunza River that drains the Karakoram batholith, platform carbonates and subordinate clastics of the Northern Karakoram Terrain and part of South Pamir to the north of the Tirich Mir-Wakhan Fault (Fig. 1B). MRS 4 was collected from the Ghizar-Gilgit River that drains the Karakoram Batholith, the southern Karakoram Metamorphic Belt, and the northern part of the Kohistan island arc. MRS 2 is from the Gilgit River which is the downstream confluence of the Hunza River and Ghizar-Gilgit River (Fig. 1B).

MRS 5 was collected from the Chitral River that drains the Hindu Kush, the Karakoram and the Kohistan island arc. MRS 9 was taken from the Kabul River, which is the downstream continuation of the Chitral River, but at this location also flows over the Indian plate Himalaya. MRS 8 was taken from the Dir River that exclusively drain the southern part of Kohistan island arc (Fig. 1B).

3.2. Zircon U-Pb Analysis

Detrital zircon U-Pb ages for MRS 3, MRS 4, MRS 5, MRS 8, and MRS 9 were acquired using the London Geochronology Centre facilities at University College London based on a New Wave 193 nm laser ablation system coupled to an Agilent 7700 quadrupole-based ICP-MS. Laser operating condition for zircon used an energy density of ca 2.5 J/cm^2 and a repetition rate of 11 Hz. Repeated measurements of external zircon standard PLESOVIC (TIMS reference age 337.13±0.37 Ma; Sláma et al., 2008) are used to correct for instrumental mass bias and depth-dependent inter-element fractionation of Pb, Th and

U and Temora (Black et al., 2003) and 91500 (Wiedenbeck et al., 2004) zircons were used as secondary age standards.

Detrital zircon U-Pb ages for MRS 2 and an aliquot of MRS 3 were acquired using the Cameca IMS-1270 ion microprobe at Centre de Recherches Pétrographiques et Géochimiques (CRPG) at Nancy, France. Analytical procedure follows the method in Deloule et al. (2002). Two aliquots of MRS 3 give the same detrital zircon U-Pb ages. Detrital zircon U-Pb ages are provided in supplementary materials (Table S1).

3.3. Muscovite $^{40}Ar/^{39}Ar$ Analysis

Optically pure (inclusion-free) grains of muscovite were hand picked. Muscovites were packed in aluminum foil, stacked in quartz tubes, shielded with Cd, and irradiated for 18 hours at the Orogen State University nuclear reactor. An in-house $^{40}Ar/^{39}Ar$ age standard, Drachenfels sanidine (DRA, 25.52 +/- 0.08 Ma) (Wijbrans et al., 1995), was used to monitor the neutron flux gradient. The analysis of single crystal muscovite following the protocol in Sun et al. (2016). The program ArArCALC2.5 was used for data reduction and age calculations (Koppers, 2002). MRS 8, draining the Kohistan Island arc only, contained no muscovite. Detrital muscovite $^{40}Ar/^{39}Ar$ ages are provided in supplementary materials (Table S2).

3.4. Inversion of $^{40}Ar/^{39}Ar$ dates to exhumation rates

We summarize and contrast four methods that have been developed for the inversion of detrital thermochronometer ages to erosion rates (Table 2) (Avdeev et al., 2011; Brandon et al., 1998; Brewer et al., 2003, 2006; Duvall et al., 2012; Garver et al., 1999; Ruhl and

Hodges, 2005; Willett and Brandon, 2013). The four methods share basic similarities in numerical calculations: (1) they assume vertical trajectories without lateral variations through which particles are exhumed towards the surface; (2) the detrital minerals found in modern river sands are considered to be representative of the drainage; and (3) the residence time of sediment-transport in the drainage basin is minimal.

The method developed by Avdeev et al (2011) allows temporal variation in erosion; whilst the other methods consider the time-averaged erosion rates (steady state) since the crystals passed through the closure isotherm. Avdeev et al. (2011) developed the approach by applying the Bayesian interpretation of probability and Markov Chain Monte Carlo algorithm in the inversion of detrital thermochronometer ages to erosion rates. The approach proposes age-elevation models with assumptions of a vertical advection path and a flat isotherm (Avdeev et al. 2011), which makes it suitable for thermochronometers with higher closure temperatures and its application to $^{40}Ar/^{39}Ar$ is highlighted in “future directions” in Avdeev et al. (2011). Comparatively, the method allows investigation of temporal variation of erosion rates and has previously been applied to large drainages (e.g. the Yellow River, Yangtze, Mekong, etc.) of the central Tibetan Plateau with apatite U-Th/He and fission track analyses (Duvall et al., 2012). We developed a new MATLAB code and applied it to implement the Bayesian inversion of detrital muscovite $^{40}Ar/^{39}Ar$ dates (Fig. 5).

The method developed by Brandon et al. (1998) investigates the spatial variation in erosion; the other three methods assume drainage-wide uniform erosion. Brandon et al. (1998) developed the approach by applying a simple one-dimensional analysis to convert detrital thermochronological ages to erosion rates. The approach has previously been applied to a modern river sand collected from the Indus river which had been previously analyzed by the zircon fission track technique (Garver et al., 1999; Cerveny et al., 1988). Later the approach has been expanded to include apatite and zircon U-Th/He, apatite and zircon fission track analysis, and $^{40}Ar/^{39}Ar$ thermochronometers (K-feldspar, biotite, muscovite, and hornblende) (Reiners and Brandon, 2006). We developed a new MATLAB code to conduct the inversion of detrital muscovite $^{40}Ar/^{39}Ar$ dates (Fig. 6) according to the methods in Brandon et al. (1998) and Willett and Brandon (2013).

Given the difference of these methods and our research interests in understanding the spatial and temporal variation in erosion of the drainage basins, we apply the Avdeev's method (Avdeev et al., 2011) and Brandon's method (Brandon et al., 1998) to the inversion of detrital muscovite $^{40}Ar/^{39}Ar$ dates to erosion rates (Table S3). We contrast results from both methods to investigate the variation in erosion of drainage basin through space and time.

4. Results and discussion

4.1 Detrital zircon U-Pb ages

The detrital zircon U-Pb ages from modern river sediments of Indus tributaries (MRS 2, MRS 3, MRS 4, MRS 5, MRS 8, and MRS 9) are presented in Figures 2 and 3 along with compiled published bedrock data from the source terranes.

As expected (see Alizai et al., 2011), the spectra from the upper Indus tributaries are distinct from those rivers draining Indian plate Himalayan formations in their significant young <200 Ma populations (Figs. 2 and 3); this reflects their drainage area encompassing the pre-collisional Andean-type subduction-related batholiths and the Kohistan island arc. The sample from the Indus River mouth has a hybrid spectrum (TH-1 in Fig. 2) representing both young ages from the upper Indus tributaries and Paleozoic-Precambrian grains which are predominant in tributaries draining the Indian plate Himalaya which is predominant in TH-1.

MRS 3 (Hunza River) drains a minor part of the Southern Karakoram Metamorphic Belt, the Karakoram Batholith and Northern Karakoram Terrain as well as the South Pamir in its upper headwaters. Its U-Pb age spectrum matches with the published compilation characteristic signature of the Karakoram and the South Pamir (Fig. 2) and it lies close to the poles of the South Asian margin (the Karakoram and South Pamir) in the multidimensional scaling plot (Fig. 4), supportive of detritus derived from these terranes. The lack of Cenozoic peak, typical of the Karakoram terrain from bedrock studies (Fig. 3), is likely due to the fact that post-collisional Cenozoic plutons are volumetrically minor, and their prevalence has been over-enhanced in the published compilation spectrum due to the focus of published research on such rocks.

MRS 4 (Ghizar-Gilgit River) drains both the Karakoram (the Southern Karakoram Metamorphic Belt as well as Karakoram Batholith) and the Kohistan arc and MRS 2 (Gilgit River) is downstream of the confluence of the Hunza River and Ghizar-Gilgit River (Fig. 1). The U-Pb zircon spectra of MRS 4 and MRS 2 resemble both the Karakoram and Kohistan arc terrains, which are in themselves very similar (Figs. 2 and 3). The greater affinity of MRS 3 and MRS 2 to the South Pamir compared to MRS 4

(Fig. 4) reflects the difference in drainage basins, with MRS 2 and 3, but not MRS 4, including the South Pamir in their catchment areas, and MRS 4 consisting of a higher percentage of Kohistan arc. This is consistent with the ~40–80 Ma peak dominant in MRS 4 which is strongly represented in MRS 8 (Dir River) (Fig. 3), which exclusively drains the Kohistan arc and shows strong affinity to the pole of Kohistan arc on the multidimensional scaling plot (Fig. 4).

MRS 5 (Chitral River) drains the Hindu Kush, the Karakoram (the Southern Karakoram Metamorphic Belt and Karakoram Batholith) and the Kohistan arc. Accordingly, its spectrum shows resemblance to these terranes, including a 200 Ma population (Fig. 3), documented thus far in the Hindu Kush only (Hildebrand et al., 2001). It has, however, an unexpected high input of Precambrian grains that results in an affinity close to the poles of terranes which are typified by such old grains in the MDS plot (Fig. 4), such as the Indian plate. Prevalence of old grains in MRS 5 may be the result of this river's long transit through a zone of sedimentary rocks in the Tirich Mir fault-Wakhan Fault Zone. The 200 Ma peak and prevalence of older grains is also observed in MRS 9 (Kabul River) (Fig. 3) draining the same terrains as MRS 5, but with the additional source downstream of the Indian plate Himalaya, which may also have contributed to the Precambrian aged zircons at the MRS 9 location. MRS 9's affinity to Asian contributions is supported by the similar detrital zircon U-Pb spectrum to that of the Upper Indus sediment sample collected at Attock (Fig. 2); MRS 9 and the Attock sample cannot be differentiated on the multidimensional scaling plot (Fig. 4).

Hildebrand et al. (2001) noted that the 200 Ma population had been recorded in the Hindu Kush, but nowhere else along the southern margin of Asia. Our data would lend support to this observation in that the two samples which have a drainage area which include the Hindu Kush (samples MRS 5 and MRS 9) contain grains of such an age, whilst the samples draining the Karakoram but not the Hindu Kush (samples MRS 2, MRS 3, and MRS 4) do not (Fig. 3). Whilst it is conceivable that such a population in these two rivers was derived from the Kohistan island arc, rather than the Hindu Kush, we think this highly improbable since: 1) such grains are rare in Kohistan (samples MRS 2, MRS 4, MRS 8); 2) samples MRS 5 and MRS 9 do not display the ~40–80 Ma peak characteristic of the Kohistan island arc, and 3) the Chitral-Kabul River's drainage basin only includes a small proportion of the Kohistan island arc.

The origin of the significant Paleogene population (30–37 Ma, peak at 35 Ma, plus a few grains at ca. 50 Ma) recorded in MRS 9 is enigmatic. The significance of the peak in the downstream MRS 9, and complete absence of a similar peak in the upstream MRS 5 might suggest that the grains come from the Indian plate Himalaya, through which the river of the downstream sample only flowed. However, only rare Paleogene granites have been recorded in the western part of the Indian plate, dated at 47 Ma (Smith et al., 1994), which is a poor match for the grains recorded here. Furthermore, if significant Indian plate input contributed to the zircon population, a concomitant increase in zircons of Precambrian and Paleozoic age would be expected.

Grains of Palaeogene age have been recorded in the Kohistan arc (e.g. Bouilhol et al., 2013; Heuberger et al., 2007), yet two lines of evidence suggest that the Kohistan arc is not the source of the grains in MRS 9: firstly, the Kohistan batholith only forms a minor part of this drainage basin for MRS 5 and MRS 9 (Fig. 1B); secondly, the appearance of these Palaeogene zircons in MRS 9 is accompanied by the first significant appearance downstream of similar aged muscovites (Fig. 3), suggesting a common source. Such aged micas are absent from the Kohistan island arc in which muscovites are rare. We therefore suggest that the most likely source for these Paleogene zircons is the Asian plate north of the arc. We suggest that the lack of such a peak in MRS 5 is the result of increasing inputs of an unidentified source from the Asian plate to MRS 9 from Afghan tributaries with unstudied drainage basin geology, joining the Kabul River downstream.

Similar aged Paleogene zircons have been also reported in the Katawaz Basin and Makran accretionary wedge to the south and the southwest of our studied area (Fig.1A); sediments in these two basins were argued to be derived from the proto-Himalayan orogen (Carter et al., 2010) or from a local source of continental arc and ophiolites from the Makran (Mohammadi et al. (2016).

4.2 Detrital muscovite $^{40}Ar/^{39}Ar$ thermochronometer

4.2.1 $^{40}Ar/^{39}Ar$ ages

We have dated 356 detrital muscovite grains. All grains are younger than 200 Ma (most < 120 Ma), except one grain from MRS 3 that has an age of 267.8 Ma (Table S2).

Samples MRS 3 and MRS 4, despite draining similar tectonic terranes (MRS 4 draining the Northern Kohistan Arc, the South Karakoram Metamorphic Belt and the Karakoram Batholith and MRS 3 draining minor part of the South Karakoram Metamorphic Belt, the

Karakoram Batholith, the Northern Karakoram Terrain and South Pamirs), show distinct detrital muscovite $^{40}Ar/^{39}Ar$ age distributions (Fig. 3). $^{40}Ar/^{39}Ar$ ages for the Ghizar-Gilgit River (MRS 4, draining northern Kohistan, the Southern Karakoram Metamorphic Belt and the Karakoram Batholith) range between 24.6 Ma and 102.5 Ma with peaks at ca. 30 Ma, 50 Ma, 70 Ma, and 100 Ma (Fig. 3). Since muscovites are extremely rare in the igneous units of the Kohistan arc (Parrish and Tirrul, 1989; Schärer et al., 1990) (e.g. MRS 8 draining only the Kohistan arc has no micas), we interpret muscovites from MRS 4 as Karakoram-derived, including the South Karakoram Metamorphic Belt and the Karakoram Batholith. These white mica $^{40}Ar/^{39}Ar$ ages are consistent with bedrock hornblende and biotite ages reported by Treloar et al (1989) from the Karakoram in the region of this river's headwaters.

By contrast, MRS 3 from the Hunza River (draining the Hunza pluton of the Karakoram Batholith, the Northern Karakoram Terrain, the South Pamir and a minor part of the Southern Karakoram Metamorphic Belt) has a range of $^{40}Ar/^{39}Ar$ ages between 4.4–32.3 Ma, and grains aged < 13 Ma are dominant (60 out of 71 grains) (Fig. 3), which is broadly consistent with the ages supplied by a range of thermochronological techniques in bedrock data from that region (Krol et al 1996b).

$^{40}Ar/^{39}Ar$ ages of MRS 2 concentrate between 3.4 Ma and 39.8 Ma with a couple of grains at 70 Ma (Fig. 3). MRS 2 is located downstream of the confluence of MRS 3 (Hunza River) and MRS 4 (Ghizar-Gilgit River); its age spectrum overlaps and shares characteristics with MRS 3 and MRS 4 but loses the age peaks of 50 Ma and 100 Ma seen in MRS4 (Fig. 3).

Most $^{40}Ar/^{39}Ar$ ages of the Chitral River MRS 5 (draining the Hindu Kush and Karakoram, and a small proportion of the Kohistan arc which does not contain muscovites) are between 110 Ma and 120 Ma with some grains around 20 Ma, 60 Ma, and 200 Ma. The downstream MRS 9, with a similar source catchment to MRS 5 with the addition of the Indian plate, has a similar range in $^{40}Ar/^{39}Ar$ age distribution (20-200 Ma) as MRS 5 but it has a major peak around 20 Ma (Fig. 3).

4.3 Exhumation rates as determined from $^{40}Ar/^{39}Ar$ muscovite ages

We have developed two MatLab codes and applied them to the inversion of detrital muscovite $^{40}Ar/^{39}Ar$ ages to erosion rates (Figs. 5 and 6). Method of Avdeev et al. (2011) focuses on the temporal variations, allowing evaluation on erosion histories, whilst the method of Brandon et al. (1998) emphasizes the spatial variation in erosion in drainage (Table 2).

4.3.1. Long-term exhumation rate variations

Numerical modeling by using the method proposed by Avdeev et al. (2011) reveals temporal variations in erosion across the Hindu Kush-Karakoram. To the first order observation, the numerical modeling results using the method of Avdeev et al. (2011) reveal the most recent and greatest erosion in the Hunza River drainage (MRS 3) in the eastern Karakoram (Fig. 5), with the micas probably derived from a catchment encompassing the Karakoram and South Pamir. The erosion rate increases from 90.9 m/Ma to 601.2 m/Ma at ca. 8.5 Ma (Fig. 5). MRS 4 from the Ghizar-Gilgit River, with muscovites interpreted as derived from the Karakoram since the Kohistan arc contains only sparse muscovites, shows a relatively high erosion rate of 186.8 m/Ma between 34.5 Ma and 24.6 Ma, and a rate of 286.3 m/Ma between 71.3 Ma and 69.6 Ma (Fig. 5).

Numerical modeling results reveal that the Chitral drainage of MRS 5 experienced one phase of fast erosion with a rate of 303.3 m/Ma between 115.2 Ma and 124.5 Ma and two phases of slow erosion before and after this period (Fig. 5; Table S3). Given the drainage basin from which this sample was collected, this most likely reflects erosion in the Hindu Kush and/or western Karakoram. The numerical modeling results for MRS 9 from the Kabul River capture a fastest period of erosion with a rate of 305.7 m/Ma starting at 27.2 Ma. Prior to this phase of fast erosion, there was a protracted period of slow erosion (8.7 m/Ma) since 125.1 Ma. An earlier phase with comparably high erosion (173.0 m/Ma) was constrained to be between 125.1–128.8Ma that follows a period of slow erosion (Fig. 5). The timing of this earlier phase of fast erosion is similar to MRS 5 but with smaller rate.

4.3.2. Spatially varying exhumation rates

Numerical calculations using the method developed by Brandon et al. (1998) give temporally averaged but spatially varying erosion rates (Fig. 6). The first order observation reveals that 1) erosion rates are lower for drainages of MRS 4 (micas derived from the Karakoram), MRS 5 (micas derived from the Hindu Kush and/or western Karakoram), and MRS 9 (downstream of MRS 5); 2) the Hunza River drainage of MRS 3 has the highest rates, with micas derived from a catchment encompassing the Karakoram and South Pamir (Fig. 6). The erosion rate varies from a few hundred meters/Ma to > 2,000 meters/Ma (2 mm/yr) for the Hunza River drainage of MRS 3. The medium value for the Hunza River drainage of MRS 3 is 1.14 mm/yr (Fig. 6), suggesting that more than half of the Hunza drainage of MRS 3 has an erosion rate > 1.14 mm/yr. By contrast, the medium erosion values for MRS 4, MRS 5, and MRS 9 are 0.15 mm/yr, 0.06 mm/yr, and 0.32 mm/yr, respectively (Fig. 6).

We note the difference in modeled erosion rates using Avdeev's method (Avdeev et al., 2011) and Brandon's method (Brandon et al., 1998); this difference is rooted in different assumptions of the two methods with one focusing on the long-term average erosion rate (Avdeev et al., 2011) and the other one estimating spatial variations in present-day rate (Brandon et al., 1998).

4.4 Temporal and spatial variations in crustal thickening and exhumation: relationships with tectonics

The earliest recorded Mesozoic crustal accretion is documented by a population of ~200 Ma detrital zircon U-Pb ages (Fig. 3) and co-eval rapid exhumations captured by detrital muscovite $^{40}Ar/^{39}Ar$ ages 179.9 Ma to 195.8 Ma of MRS 5 and MRS 9 which partially drain the Hindu Kush. Hildebrand et al. (2001) noted that zircons of such age have not yet been recorded in the Karakoram, an observation which is upheld by our new data from the Karakoram-draining rivers (MRS 2, 3, and 4). Previous work recording such ages are restricted in the Hindu Kush to monazites from the Garam Chashma pluton (Faisal et al., 2014; Hildebrand et al., 2001), located close to MRS 5. Faisal et al. (2014) record monazite populations dated between 211 +/- 7.9 to 201.5 +/- 3.6 Ma and 189.7 +/- 4.8 to 184.6 +/- 3.4 Ma, which they interpret as either reflecting a single protracted metamorphic event, or two events, related first to the collision of the Hindu Kush with the Central Pamir along the Rushan-Pshart Suture, and then to the collision of the

Karakoram with the Hindu Kush along the Tirich Mir-Wakhan Fault zone. Detrital zircon U-Pb ages of ~200 Ma from MRS 5 and MRS 9, covering a period from 190.8 +/- 2.8 to 212.4 +/- 2.7 Ma, overlap these two previously recorded age populations. We speculate that the presence of ca. 200 Ma population in the Hindu Kush (also recorded in the correlative South Pamir, e.g. Blayney et al 2016), but its lack of documentation, to date, in the Karakoram (see section 4.1), may be the result of the docking of the Hindu Kush – South Pamir terrane with the Central Pamir at this time, closely followed by the closure of the basin between the Hindu Kush and Karakoram along the Tirich Mir-Wakhan Fault zone to the south (Angiolini et al., 2013; Robinson, 2015; Zanchi et al., 2000).

Zircons <200 Ma reflect the ongoing closure of Neotethys culminating in the eventual collision of India with Asia. All samples draining the Karakoram and Hindu Kush show a dominant peak of detrital zircon U-Pb ages at ca. 100–120 Ma (Fig. 3). This is consistent with previous work documenting similar zircon and monazite ages (95–130 Ma) in both terranes (e.g. Debon et al., 1987; Fraser et al., 2001; Heuberger et al., 2007), which is related to the subduction of Neotethys beneath the southern margin of the Andean-style margin of Asia. Two phases of fast erosion at ca. 115–124 Ma and 125–129 Ma, modeled in the MRS 5 and MRS 9 of the Chitral and Kabul river samples, overlap zircon and monazite ages and likely represent a single protracted phase of accelerating erosion across the South Asian margin of the Hindu Kush/Karakoram, related to the same subduction system. Additional evidence of fast erosion in the Hindu Kush at this time comes from the Cretaceous Reshun conglomerate unit in the Tirich Mir fault zone; its existence implies that the Hindu Kush was acting as an active source during the deposition of this conglomerate (Pudsey et al., 1985). Early Cretaceous subduction and accretion processes were also widely observed in the Karakoram (e.g. Alizai et al., 2011; Hildebrand et al., 2001; Searle and Tirrul, 1991; Searle, 1991); the evidence includes U-Pb dating on the Hushe gneiss, Hunza granodiorite, and K2 gneiss that constrained the subduction and accretion events to be between 100 Ma and 140 Ma and the synorogenic Tupop conglomerate unit which was deposited in the northern Karakoram (Gaetani et al., 1993) in response to the orogenic processes of the active Asian margin (Hildebrand et al., 2001). According to Faisal et al. (2014), the Early Cretaceous subduction ceased at the location described above, in the Late Cretaceous, due to collision of the Kohistan Island arc with the Asian margin at ~85–90 Ma. They interpret monazite ages of 88 and 72 Ma in the Hindu Kush as the result of the re-establishment of the subduction zone to the south. A scarcity of zircon ages in the range of ~80–90 Ma for all of our Hindu Kush- and Karakoram-draining samples may reflect this southerly jump in the location of subduction. The comparatively high erosion rate (286.3 m/Ma) at 69–71 Ma from MRS 4 (Fig. 5) might reflect this collision-related erosion in the Southern Karakoram Metamorphic Belt.

Our oldest recorded accelerating erosions post India-Asia collision start at 35 Ma (MRS 4; micas derived from the Karakoram) with muscovites of the same age also recorded in MRS 5) from the Kabul River, which we interpret as associated with the 30–37 Ma zircon U-Pb ages in MRS 9 (Table S2). This is followed by a second accelerated erosion at 27 Ma (MRS 9; micas derived from the Hindu Kush and Karakoram). Additionally, MRS 5 has a small peak of detrital muscovite $^{40}Ar/^{39}Ar$ ages between ca. 18 Ma and 28 Ma (five grains; Table S3), possibly linked to fast erosion at this time in Chitral River drainage although the numerical modeling did not capture this signal due to the preponderance of ~120 Ma aged grains (Figs. 3 and 5).

In contrast to MRS 4's youngest record of exhumation at 35 Ma (Fig 5, Table S3) and youngest mica age / peak of 25 and 30 Ma respectively, MRS 3, along strike to the East, with a catchment draining the Karakoram and South Pamir, has a very different mica age distribution and exhumation pattern. MRS 3 displays the most recent intense exhumation of all our samples, as reflected in the concentration of young detrital muscovite $^{40}Ar/^{39}Ar$ ages (youngest age: 4.4 Ma; 61 out of 71 grains younger than 13 Ma, Table S2; Fig. 3), and the modeled fastest erosion rate (601.2m/Ma at 8.5 Ma) (Fig. 5; Table S3).

We consider that the difference in mica ages and periods of rapid exhumation between samples MRS 3 and 4, along-strike in the Karakoram may be the result of either: (1) proximity of MRS 3 river's headwaters to the Karakoram Fault, along which young exhumation, of similar age to the 8 Ma accelerated erosion we document, has already been recorded at a number of locations (e.g. Dunlap et al., 1998; Wallis et al., 2016), or (2) along-strike variation in the tectonics of the Karakoram. Both Searle et al (2010) and Palin et al (2012) noted differences between the western (Hunza) and eastern (Baltoro) regions in terms of their metamorphic and magmatic histories. This difference they ascribed to either diachroneity of evolution along strike in the Karakoram, or variation in the degree of exhumation. Our data from the Hunza River may indicate that the Late Miocene rapid exhumation experienced in the Baltoro Region of the Karakoram (Cerveny et al., 1989; Foster et al., 1994) extends at least as far west as the eastern part of

Hunza, consistent with the work of Krol et al, (1996b). More exhumational data from further west is required to investigate this question further.

Wallis et al. (2016) previously discussed spatial variations in the region. They noted a northward decrease in mineral exhumation age and increase in exhumation rate across the Indus suture zone from the Ladakh batholith to the Eastern Karakoram. They proposed a driving force related to the crustal thickening-driven uplift, subsequent creation of great relief and development of glaciation for the late Miocene rapid exhumation seen in the eastern Karakoram. Our data would indicate that this late Miocene-Pliocene rapid exhumation extended as far west as the Hunza River, if the locus of our recorded rapid exhumation in the Hunza River sample MRS 3 is taken to be the Karakoram Batholith rather than the region of the Karakoram Fault in the river's headwaters.

Our recorded rapid exhumation in the Karakoram at 8.5 Ma is observed downstream in the foreland basin. Chirouze et al. (2015) conducted a study of bulk trace element and Hf-Nd isotopes, and detrital zircon fission track analyses on modern Indus and paleo-Indus deposits in the western Himalayan foreland. Their results indicate increasing contribution of inputs from the Karakoram to the late Miocene Siwalik sediments, consistent with our documentation of increased exhumation from the Karakoram at this time.

5. Conclusions

Our zircon and mica data and modelled erosion rates contribute further to the growing dataset that map the extent to which the present-day topography in this region is a result of not only post– but also pre- India-Asia collision, long-term crustal accretion, shortening, and thickening, which started with the Mesozoic amalgamation of the various Gondwanan terranes. Our data from the Karakoram-Hindu Kush regions show a) further support to the suggestion that the ca. 200 Ma old detrital zircon population present in the Hindu Kush is absent from the Karakoram, and may reflect the collision between the Hindu Kush-South Pamir with Central Pamir, b) a dominant arc-derived peak of detrital zircon U-Pb ages at ca. 120 Ma in all MRS samples, and c) fast erosion pre-India-Asia collision at 115–128 Ma and 71 Ma. However, India-Asia collision is the most pervasive factor affecting erosion rate, as evidenced by post-collision fast erosion periods recorded at 35 Ma, 27 Ma and 8.5 Ma. There is also significant spatial variation in exhumation, in particular the rapid exhumation at 8 Ma is only observed furthest east in our study area. Such a variation may reflect east-west along-strike variation in exhumation, as previously documented with respect to metamorphic and magmatic episodes, or the proximity of the Hunza River headwaters to the Karakoram Fault.

Acknowledgements

Financial support was provided under the Initial Training Network iTECC by the EU REA under the FP7 implementation of the Marie Curie Action (grant # 316966). We thank Xiaobin Cao on probability calculations and Mark Brandon for discussions on the interpretation of detrital thermochronometric dates. Etienne Deloule, Michel Champenois, Gwladys Govin, and Jesse Davenport are acknowledged for help during detrital zircon U-Pb analysis at CRPG (CNRS).

Figure Captions

Figure 1. (A) Topographic map of western part of Himalaya and Tibetan Plateau with the Indus drainage. Collection sites of modern river sediment samples (MRS 2, 3, 4, 5, 8, and 9, this study) are indicated by white solid circles. Purple (blue) solid circles indicate previous sampling sites of Himalaya tributary river sediments (a–g) (Alizai et al., 2011), and modern river sediments at the Indus River mouth (TH-1) (Clift et al., 2004)**. (B)** Topographic map superimposed with simplified geology and the Upper Indus shown with tributaries and sample locations of modern river sediment (MRS) samples. Main Karakoram Thrust (MKT) / Shyok Suture Zone (SSZ), Main Mantle Thrust (MMT) / Indus Suture Zone (ISZ).

Figure 2. Cumulative curves of modern river sediments of the Upper Indus tributaries (MRS 2, 3, 4, 5, 8, and 9; this study), Himalayan tributaries (a–g) (Alizai et al., 2011), and Indus River mouth sample TH-1 (Clift et al., 2004). **(B)** Probability density curves of detrital zircon U-Pb dates of potential source terranes. We compiled and grouped detrital zircon U-Pb ages from previous publications for Kohistan-Ladakh oceanic arcs (Bosch et al., 2011; Bouilhol et al., 2011, 2013; Clift and Gaedicke, 2002; Henderson et al., 2011; Heuberger et al., 2007; Honegger et al., 1982; Jagoutz et al., 2009; Khan et al., 2009; Krol et al., 1996a; Ravikant et al., 2009; Schärer et al., 1984; Singh et al., 2007; St-Onge et al., 2010; Upadhyay et al., 2008; Weinberg et al., 2000; White et al., 2011), Karakoram (Fraser et al., 2001; Heuberger et al., 2007; Jain and Singh, 2008; Mahar et al., 2014; Parrish and Tirrul, 1989; Phillips et al., 2004; Ravikant et al., 2009; Schärer et al., 1990; Searle et al., 1998; Sen et al., 2014; Weinberg et al., 2000), Hindu Kush (Hildebrand et al., 1998; Hildebrand et al., 2001), and South Pamir (Blayney et al., 2016). Detrital zircon

U-Pb ages for terrains of Tethyan Himalaya, Lesser Himalaya, and Higher Himalaya are compiled from Clift et al., (2014), Gehrels et al. (2003, 2008), and Hu et al. (2010).

Figure 3. (A-F) Histograms of detrital muscovite ^{40}Ar/^{39}Ar ages and detrital zircon U-Pb ages (0~240 Ma). Note MRS 8 draining the Kohistan arc exclusively has no muscovites. **(G)** Kernel Density Estimation (KDE) (Vermeesch, 2012) plot of compiled detrital zircon U-Pb ages of potential source terranes. For cited references of potential source terranes, refer to Figure 2 caption.

Figure 4. A multidimensional scaling plot (Vermeesch, 2013) displays the similarities/dissimilarities between the modern river sediment samples (MRS 2, 3, 4, 5, 8, and 9, this study; Himalaya tributaries, Alizai et al., 2011; lower Indus TH1, Clift et al., 2004) and potential source terranes (Lesser Himalaya–LH, Higher Himalaya–HH, Tethyan Himalaya–TH; Asian margin, including Karakoram–KK, Hindu-Kush–HK, and South Pamir–SP; Kohistan Island Arc–KLA). For cited references for potential source terranes, refer to Figure 2 caption.

Figure 5. Model results of MRS samples, obtained by applying new MATLAB code to implement Avdeev method (Avdeev et al., 2011) allowing variations in erosion time through time (discrete segments in elevation versus age profiles). **(Left column; A, D, G, J)** Plots of detrital muscovite ^{40}Ar/^{39}Ar age (Ma) against elevation (km). Dashed (black) line represents the best (average) model. **(Middle column; B, E, H, K)** Cumulative probability density plots showing actual ages (open circles) and synthetic ages modeled from the best model (dashed line) and the average model (solid line). **(Right column; C, F, I, L)** Plots of erosion rate versus time (Ma).

Figure 6. Model results obtained by applying the method of Brandon et al. (1998). **(Left column; a, d, g, j, m)** Kernel Density Estimation (KDE) (Vermeesch, 2012) and histogram plots of detrital muscovite $^{40}Ar/^{39}Ar$ age (Ma). **(Middle column; b, e, h, k, n)** Kernel Density Estimation (KDE) (Vermeesch, 2012) and histogram plots of modeled erosion rates (km/Ma). **(Right column; c, f, i, l, o)** Cumulative plot of modeled erosion rates shown with the medium value.

Table 1. Sample collection site coordinates, draiange, and tectonic terranes.

Table 2. Summary of methods for the inversion of detrital thermochronometer ages to erosion rates.

Cited References

1. Aitchison, J.C., Ali, J.R., Davis, A.M., 2007. When and where did India and Asia collide? Journal of Geophysical Research: doi:10.1029/2006JB004706.
2. Alizai, A., Carter, A., Clift, P.D., VanLaningham, S., Williams, J.C., Kumar, R., 2011. Sediment provenance, reworking and transport processes in the Indus River by U–Pb dating of detrital zircon grains. Global and Planetary Change 76, 33-55.
3. Angiolini, L., Zanchi, A., Zanchetta, S., Nicora, A., Vezzoli, G., 2013. The Cimmerian geopuzzle: new data from South Pamir. Terra Nova 25, 352-360.
4. Avdeev, B., Niemi, N.A., Clark, M.K., 2011. Doing more with less: Bayesian estimation of erosion models with detrital thermochronometric data. Earth and Planetary Science Letters 305, 385-395.

5. Black, L.P., Kamo, S.L., Allen, C.M., Aleinikoff, J.N., Davis, D.W., Korsch, R.J., Foudoulis, C., 2003. TEMORA 1: a new zircon standard for Phanerozoic U–Pb geochronology. Chemical Geology 200, 155-170.

6. Blayney, T., Najman, Y., Dupont‐Nivet, G., Carter, A., Miller, I., Garzanti, E., Sobel, E.R., Rittner, M., Ando, S., Guo, Z., 2016. Indentation of the Pamirs with respect to the northern margin of Tibet: constraints from the Tarim Basin sedimentary record. Tectonics, 35, 2345–2369, doi:10.1002/2016TC004222.

7. Bosch, D., Garrido, C.J., Bruguier, O., Dhuime, B., Bodinier, J.-L., Padròn-Navarta, J.A., Galland, B., 2011. Building an island-arc crustal section: Time constraints from a LA-ICP-MS zircon study. Earth and Planetary Science Letters 309, 268-279.

8. Boutonnet, E., Leloup, P., Arnaud, N., Paquette, J.L., Davis, W., Hattori, K., 2012. Synkinematic magmatism, heterogeneous deformation, and progressive strain localization in a strike-slip shear zone: The case of the right-lateral Karakorum fault. Tectonics 31, 10.1029/2011TC003049.

9. Bouilhol, P., Jagoutz, O., Hanchar, J.M., Dudas, F.O., 2013. Dating the India–Eurasia collision through arc magmatic records. Earth and Planetary Science Letters 366, 163-175.

10. Bouilhol, P., Schaltegger, U., Chiaradia, M., Ovtcharova, M., Stracke, A., Burg, J.-P., Dawood, H., 2011. Timing of juvenile arc crust formation and evolution in the Sapat Complex (Kohistan–Pakistan). Chemical Geology 280, 243-256.

11. Brandon, M.T., Roden-Tice, M.K., Garver, J.I., 1998. Late Cenozoic exhumation of the Cascadia accretionary wedge in the Olympic Mountains, northwest Washington State. Geological Society of America Bulletin 110, 985-1009.

12. Braun, J., Van Der Beek, P., Batt, G., 2006. Quantitative thermochronology: numerical methods for the interpretation of thermochronological data. Cambridge University Press.

13. Brewer, I., Burbank, D., Hodges, K., 2003. Modelling detrital cooling ‐ age populations: Insights from two Himalayan catchments. Basin Research 15, 305-320.

14. Brewer, I., Burbank, D., Hodges, K., 2006. Downstream development of a detrital cooling-age signal: Insights from $^{40}Ar/^{39}Ar$ muscovite thermochronology in the Nepalese Himalaya. Geological Society of America Special Papers 398, 321-338.

15. Brozović, N., Burbank, D.W., Meigs, A.J., 1997. Climatic limits on landscape development in the northwestern Himalaya. Science 276, 571-574.

16. Carter, A., Najman, Y., Bahroudi, A., Bown, P., Garzanti, E., Lawrence, R.D., 2010. Locating earliest records of orogenesis in western Himalaya: Evidence from Paleogene sediments in the Iranian Makran region and Pakistan Katawaz basin. Geology 38, 807-810.

17. Cerveny, P.F., Naeser, C.W., Kelemen, P.B., Lieberman, J.E., Zeitler, P.K., 1989. Zircon fission-track ages from the Gasherbrum Diorite, Karakoram Range, northern Pakistan. Geology 17, 1044-1048.

18. Cerveny, P., Naeser, N., Zeitler, P., Naeser, C., Johnson, N., 1988. History of uplift and relief of the Himalaya during the past 18 million years: Evidence from

fission-track ages of detrital zircons from sandstones of the Siwalik Group, New perspectives in basin analysis. Springer, pp. 43-61.

19. Chirouze, F., Huyghe, P., Chauvel, C., van der Beek, P., Bernet, M., Mugnier, J.-L., 2015. Stable Drainage Pattern and Variable Exhumation in the Western Himalaya since the Middle Miocene. The Journal of Geology 123, 1-20.

20. Clift, P.D., Campbell, I.H., Pringle, M.S., Carter, A., Zhang, X., Hodges, K.V., Khan, A.A., Allen, C.M., 2004. Thermochronology of the modern Indus River bedload: New insight into the controls on the marine stratigraphic record. Tectonics 23 doi:10.1029/2003TC001559.

21. Clift, P.D., Carter, A., Jonell, T.N., 2014. U–Pb dating of detrital zircon grains in the Paleocene Stumpata Formation, Tethyan Himalaya, Zanskar, India. Journal of Asian Earth Sciences 82, 80-89.

22. Clift, P.D., Gaedicke, C., 2002. Accelerated mass flux to the Arabian Sea during the middle to late Miocene. Geology 30, 207-210.

23. Debon, F., Le Fort, P., Dautel, D., Sonet, J., Zimmermann, J., 1987. Granites of western Karakorum and northern Kohistan (Pakistan): a composite Mid-Cretaceous to upper Cenozoic magmatism. Lithos 20, 19-40.

24. DeCelles, P., Kapp, P., Gehrels, G., Ding, L., 2014. Paleocene‐Eocene foreland basin evolution in the Himalaya of southern Tibet and Nepal: Implications for the age of initial India‐Asia collision. Tectonics 33, 824-849.

25. Deloule, E., Alexandrov, P., Cheilletz, A., Laumonier, B., Barbey, P., 2002. In-situ U-Pb zircon ages for Early Ordovician magmatism in the eastern Pyrenees,

France: the Canigou orthogneisses. International Journal of Earth Sciences 91, 398-405.

26. DiPietro, J.A., Pogue, K.R., 2004. Tectonostratigraphic subdivisions of the Himalaya: A view from the west. Tectonics 23, DOI: 10.1029/2003TC001554.

27. Dunlap, W.J., Weinberg, R.F., Searle, M.P., 1998. Karakoram fault zone rocks cool in two phases. Journal of the Geological Society 155, 903-912.

28. Duvall, A.R., Clark, M.K., Avdeev, B., Farley, K.A., Chen, Z., 2012. Widespread late Cenozoic increase in erosion rates across the interior of eastern Tibet constrained by detrital low-temperature thermochronometry. Tectonics 31 doi:10.1029/2011TC002969.

29. Faisal, S., Larson, K.P., Cottle, J.M., Lamming, J., 2014. Building the Hindu Kush: Monazite Records of Terrane Accretion, Plutonism, and the Evolution of the Himalaya–Karakoram–Tibet Orogen. Terra Nova 26, 395-401.

30. Foster, D.A., Gleadow, A.J., Mortimer, G., 1994. Rapid Pliocene exhumation in the Karakoram (Pakistan), revealed by fission-track thermochronology of the K2 gneiss. Geology 22, 19-22.

31. Fraser, J.E., Searle, M.P., Parrish, R.R., Noble, S.R., 2001. Chronology of deformation, metamorphism, and magmatism in the southern Karakoram Mountains. Geological Society of America Bulletin 113, 1443-1455.

32. Gaetani, M., Garzanti, E., 1991. Multicyclic history of the Northern India continental margin (Northwestern Himalaya) (1). AAPG Bulletin 75, 1427-1446.

33. Gaetani, M., Jadoul, F., Erba, E., Garzanti, E., 1993. Jurassic and Cretaceous orogenic events in the North Karakoram: age constraints from sedimentary rocks. Geological Society, London, Special Publications 74, 39-52.

34. Garver, J.I., Brandon, M.T., Roden-Tice, M., Kamp, P.J., 1999. Exhumation history of orogenic highlands determined by detrital fission-track thermochronology. Geological Society, London, Special Publications 154, 283-304.

35. Gehrels, G., DeCelles, P., Martin, A., Ojha, T., Pinhassi, G., Upreti, B., 2003. Initiation of the Himalayan orogen as an early Paleozoic thin-skinned thrust belt. GSA today 13, 4-9.

36. Gehrels, G.E., Valencia, V.A., Ruiz, J., 2008. Enhanced precision, accuracy, efficiency, and spatial resolution of U-Pb ages by laser ablation–multicollector–inductively coupled plasma–mass spectrometry. Geochemistry, Geophysics, Geosystems 9, Q03017, doi:10.1029/2007GC001805.

37. Henderson, A.L., Najman, Y., Parrish, R., Mark, D.F., Foster, G.L., 2011. Constraints to the timing of India–Eurasia collision; a re-evaluation of evidence from the Indus Basin sedimentary rocks of the Indus–Tsangpo Suture Zone, Ladakh, India. Earth-Science Reviews 106, 265-292.

38. Heuberger, S., Schaltegger, U., Burg, J.-P., Villa, I.M., Frank, M., Dawood, H., Hussain, S., Zanchi, A., 2007. Age and isotopic constraints on magmatism along the Karakoram-Kohistan Suture Zone, NW Pakistan: Evidence for subduction and continued convergence after India-Asia collision. Swiss Journal of Geosciences 100, 85-107.

39. Hildebrand, P., Noble, S., Searle, M., Parrish, R., 1998. Tectonic significance of 24 Ma crustal melting in the eastern Hindu Kush, Pakistan. Geology 26, 871-874.

40. Hildebrand, P., Noble, S., Searle, M., Waters, D., Parrish, R., 2001. Old origin for an active mountain range: Geology and geochronology of the eastern Hindu Kush, Pakistan. Geological Society of America Bulletin 113, 625-639.

41. Hildebrand, P., Searle, M., Khan, Z., Van Heijst, H., 2000. Geological evolution of the Hindu Kush, NW Frontier Pakistan: active margin to continent-continent collision zone. Geological Society, London, Special Publications 170, 277-293.

42. Honegger, K., Dietrich, V., Frank, W., Gansser, A., Thöni, M., Trommsdorff, V., 1982. Magmatism and metamorphism in the Ladakh Himalayas (the Indus-Tsangpo suture zone). Earth and Planetary Science Letters 60, 253-292.

43. Hu, X., Garzanti, E., Wang, J., Huang, W., An, W., Webb, A., 2016. The timing of India-Asia collision onset–Facts, theories, controversies. Earth-Science Reviews 160, 264-299.

44. Hu, X., Jansa, L., Chen, L., Griffin, W.L., O'Reilly, S.Y., Wang, J., 2010. Provenance of Lower Cretaceous Wölong volcaniclastics in the Tibetan Tethyan Himalaya: Implications for the final breakup of eastern Gondwana. Sedimentary Geology 223, 193-205.

45. Jagoutz, O.E., Burg, J.-P., Hussain, S., Dawood, H., Pettke, T., Iizuka, T., Maruyama, S., 2009. Construction of the granitoid crust of an island arc part I: geochronological and geochemical constraints from the plutonic Kohistan (NW Pakistan). Contributions to Mineralogy and Petrology 158, 739-755.

46. Jain, A.K., Singh, S., 2008. Tectonics of the southern Asian Plate margin along the Karakoram Shear Zone: Constraints from field observations and U–Pb SHRIMP ages. Tectonophysics 451, 186-205.

47. Khan, S.D., Walker, D.J., Hall, S.A., Burke, K.C., Shah, M.T., Stockli, L., 2009. Did the Kohistan-Ladakh island arc collide first with India? Geological Society of America Bulletin 121, 366-384.

48. Koppers, A.A., 2002. ArArCALC—software for $^{40}Ar/^{39}Ar$ age calculations. Computers & Geosciences 28, 605-619.

49. Krol, M.A., Zeitler, P.K., Copeland, P., 1996a. Episodic unroofing of the Kohistan Batholith, Pakistan: Implications from K-feldspar thermochronology. Journal of Geophysical Research: Solid Earth (1978–2012) 101, 28149-28164.

50. Krol, M.A., Zeitler, P.K., Poupeau, G., Pecher, A., 1996b. Temporal variations in the cooling and denudation history of the Hunza plutonic complex, Karakoram Batholith, revealed by $^{40}Ar/^{39}Ar$ thermochronology. Tectonics 15, 403-415.

51. Mahar, M.A., Mahéo, G., Goodell, P.C., Pavlis, T.L., 2014. Age and origin of post collision Baltoro granites, south Karakoram, North Pakistan: Insights from in-situ U–Pb, Hf and oxygen isotopic record of zircons. Lithos 205, 341-358.

52. Mahéo, G., Guillot, S., Blichert-Toft, J., Rolland, Y., Pêcher, A., 2002. A slab breakoff model for the Neogene thermal evolution of South Karakorum and South Tibet. Earth and Planetary Science Letters 195, 45-58.

53. McDougall, I., Harrison, T.M., 1999. Geochronology and Thermochronology by the $^{40}Ar/^{39}Ar$ Method. Oxford University Press.

54. Mohammadi, A., Burg, J.-P., Winkler, W., Ruh, J., von Quadt, A., 2016. Detrital zircon and provenance analysis of Late Cretaceous− Miocene onshore Iranian Makran strata: Implications for the tectonic setting. Geological Society of America Bulletin, v. 128, p. 1481–1499, doi: 10.1130/B31361.1.

55. Mukherjee, B.K., Sen, K., Sachan, H.K., Paul, S.K., 2012. Exhumation history of the Karakoram fault zone mylonites: New constraints from microstructures, fluid inclusions, and 40 Ar-39 Ar analyses. Lithosphere 4, 230-241.

56. Najman, Y., Jenks, D., Godin, L., Boudagher-Fadel, M., Millar, I., Garzanti, E., Horstwood, M., Bracciali, L., 2017. The Tethyan Himalayan detrital record shows that India–Asia terminal collision occurred by 54 Ma in the Western Himalaya. Earth and Planetary Science Letters 459, 301-310.

57. Palin, R., Searle, M., Waters, D., Horstwood, M., Parrish, R., 2012. Combined thermobarometry and geochronology of peraluminous metapelites from the Karakoram metamorphic complex, North Pakistan; New insight into the tectonothermal evolution of the Baltoro and Hunza Valley regions. Journal of Metamorphic Geology 30, 793-820.

58. Parrish, R.R., Tirrul, R., 1989. U-Pb age of the Baltoro granite, northwest Himalaya, and implications for monazite U-Pb systematics. Geology 17, 1076-1079.

59. Petterson, M.G., Windley, B.F., 1985. Rb-Sr dating of the Kohistan arc-batholith in the Trans-Himalaya of north Pakistan, and tectonic implications. Earth and Planetary Science Letters 74, 45-57.

60. Phillips, R.J., Parrish, R.R., Searle, M.P., 2004. Age constraints on ductile deformation and long-term slip rates along the Karakoram fault zone, Ladakh. Earth and Planetary Science Letters 226, 305-319.

61. Pudsey, C., Coward, M., Luff, I., Shackleton, R., Windley, B., Jan, M., 1985. Collision zone between the Kohistan arc and the Asian plate in NW Pakistan. Transactions of the Royal Society of Edinburgh: Earth Sciences 76, 463-479.

62. Ravikant, V., Wu, F.-Y., Ji, W.-Q., 2009. Zircon U–Pb and Hf isotopic constraints on petrogenesis of the Cretaceous–Tertiary granites in eastern Karakoram and Ladakh, India. Lithos 110, 153-166.

63. Reiners, P.W., Brandon, M.T., 2006. Using thermochronology to understand orogenic erosion. Annu. Rev. Earth Planet. Sci. 34, 419-466.

64. Robinson, A.C., 2015. Mesozoic tectonics of the Gondwanan terranes of the Pamir plateau. Journal of Asian Earth Sciences 102, 170-179.

65. Ruhl, K., Hodges, K., 2005. The use of detrital mineral cooling ages to evaluate steady state assumptions in active orogens: An example from the central Nepalese Himalaya. Tectonics 24, TC4015, doi:10.1029/2004TC001712.

66. Schärer, U., Copeland, P., Harrison, T.M., Searle, M.P., 1990. Age, cooling history, and origin of post-collisional leucogranites in the Karakoram Batholith; a multi-system isotope study. The Journal of Geology, 233-251.

67. Schärer, U., Hamet, J., Allègre, C.J., 1984. The Transhimalaya (Gangdese) plutonism in the Ladakh region: a U Pb and Rb Sr study. Earth and Planetary Science Letters 67, 327-339.

68. Schneider, D., Zeitler, P., Kidd, W., Edwards, M., 2001. Geochronologic constraints on the tectonic evolution and exhumation of Nanga Parbat, western Himalaya syntaxis, revisited. The Journal of Geology 109, 563-583.

69. Searle, M.P., 2015. Mountain building, tectonic evolution, rheology and crustal flow in the Himalaya, Karakorum and Tibet. Treatise on Geophysics 6, 469-511.

70. Searle, M.P., Khan, M.A., Fraser, J., Gough, S., Jan, M.Q., 1999. The tectonic evolution of the Kohistan ‐ Karakoram collision belt along the Karakoram Highway transect, north Pakistan. Tectonics 18, 929-949.

71. Searle, M.P., Parrish, R.R., Thow, A., Noble, S., Phillips, R., Waters, D., 2010. Anatomy, age and evolution of a collisional mountain belt: the Baltoro granite batholith and Karakoram Metamorphic Complex, Pakistani Karakoram. Journal of the Geological Society 167, 183-202.

72. Searle, M.P., Tirrul, R., 1991. Structural and thermal evolution of the Karakoram crust. Journal of the Geological Society 148, 65-82.

73. Searle, M.P., Windley, B., Coward, M., Cooper, D., Rex, A., Rex, D., Tingdong, L., Xuchang, X., Jan, M.Q., Thakur, V., 1987. The closing of Tethys and the tectonics of the Himalaya. Geological Society of America Bulletin 98, 678-701.

74. Searle, M.P., 1991. Geology and tectonics of the Karakoram Mountains. John Wiley & Sons Inc.

75. Searle, M.P., Weinberg, R.E and Dunlap, W. J., 1998. Transpressional tectonics along the Karakoram fault zone, northern Ladakh: constraints on Tibetan extrusion. In: Holdsworth, R.E., Strachan, R.A. and Dewey, J. E (eds) 1998.

Continental Transpressional and Transtensional Tectonics. Geological Society, London, Special Publications, 135, 307-326.

76. Sen, K., Mukherjee, B.K., Collins, A.S., 2014. Interplay of deformation and magmatism in the Pangong Transpression Zone, eastern Ladakh, India: Implications for remobilization of the trans-Himalayan magmatic arc and initiation of the Karakoram Fault. Journal of Structural Geology 62, 13-24.

77. Şengör, A.C., 1984. The Cimmeride orogenic system and the tectonics of Eurasia. Geological Society of America Special Papers 195, 1-74.

78. Singh, S., Kumar, R., Barley, M.E., Jain, A., 2007. SHRIMP U–Pb ages and depth of emplacement of Ladakh Batholith, Eastern Ladakh, India. Journal of Asian Earth Sciences 30, 490-503.

79. Sláma, J., Košler, J., Condon, D.J., Crowley, J.L., Gerdes, A., Hanchar, J.M., Horstwood, M.S., Morris, G.A., Nasdala, L., Norberg, N., 2008. Plešovice zircon—a new natural reference material for U–Pb and Hf isotopic microanalysis. Chemical Geology 249, 1-35.

80. Smith, H.A., Chamberlain, C.P., Zeitler, P.K., 1994. Timing and duration of Himalayan metamorphism within the Indian plate, northwest Himalaya, Pakistan. The Journal of Geology, 493-508.

81. St-Onge, M.R., Rayner, N., Searle, M.P., 2010. Zircon age determinations for the Ladakh batholith at Chumathang (Northwest India): implications for the age of the India–Asia collision in the Ladakh Himalaya. Tectonophysics 495, 171-183.

82. Sun, X., Li, C.a., Kuiper, K., Zhang, Z., Gao, J., Wijbrans, J., 2016. Human impact on erosion patterns and sediment transport in the Yangtze River. Global and Planetary Change 143, 88-99.

83. Tahirkheli, R., Mattauer, M., Proust, F., Tapponnier, P., 1979. The India Eurasia suture zone in northern Pakistan: Some new date for an interpretation at plate scale. In: Farah, A., DeJong, K.A. (eds) Geodynamics of Pakistan. Geological Survey of Pakistan, Quetta, 130-135.

84. Treloar, P.J., Izatt, C.N., 1993. Tectonics of the Himalayan collision between the Indian plate and the Afghan block: A synthesis. Geological Society, London, Special Publications 74, 69-87.

85. Treloar, P.J., Rex, D., Guise, P., Coward, M., Searle, M., Windley, B., Petterson, M., Jan, M.Q., Luff, I., 1989. K-Ar and Ar-Ar geochronology of the Himalayan collision in NW Pakistan: Constraints on the timing of suturing, deformation, metamorphism and uplift. Tectonics 8, 881-909.

86. Upadhyay, R., Frisch, W., Siebel, W., 2008. Tectonic implications of new U–Pb zircon ages of the Ladakh batholith, Indus suture zone, northwest Himalaya, India. Terra Nova 20, 309-317.

87. Van Der Beek, P., Van Melle, J., Guillot, S., Pêcher, A., Reiners, P.W., Nicolescu, S., Latif, M., 2009. Eocene Tibetan plateau remnants preserved in the northwest Himalaya. Nature Geoscience 2, 364-368.

88. van Hinsbergen, D.J., Lippert, P.C., Dupont-Nivet, G., McQuarrie, N., Doubrovine, P.V., Spakman, W., Torsvik, T.H., 2012. Greater India Basin

hypothesis and a two-stage Cenozoic collision between India and Asia. Proceedings of the National Academy of Sciences 109, 7659-7664.

89. Vermeesch, P., 2012. On the visualisation of detrital age distributions. Chemical Geology 312, 190-194.

90. Vermeesch, P., 2013. Multi-sample comparison of detrital age distributions. Chemical Geology 341, 140-146.

91. Wallis, D., Carter, A., Phillips, R.J., Parsons, A.J., Searle, M.P., 2016. Spatial variation in exhumation rates across Ladakh and the Karakoram: New apatite fission track data from the Eastern Karakoram, NW India. Tectonics 35, 704-721.

92. Weinberg, R., Dunlap, W., Whitehouse, M., 2000. New field, structural and geochronological data from the Shyok and Nubra valleys, northern Ladakh: linking Kohistan to Tibet. Geological Society, London, Special Publications 170, 253-275.

93. White, L., Ahmad, T., Ireland, T., Lister, G., Forster, M., 2011. Deconvolving episodic age spectra from zircons of the Ladakh Batholith, northwest Indian Himalaya. Chemical Geology 289, 179-196.

94. Wiedenbeck, M., Hanchar, J.M., Peck, W.H., Sylvester, P., Valley, J., Whitehouse, M., Kronz, A., Morishita, Y., Nasdala, L., Fiebig, J., 2004. Further characterisation of the 91500 zircon crystal. Geostandards and Geoanalytical Research 28, 9-39.

95. Wijbrans, J., Pringle, M., Koppers, A., Scheveers, R., 1995. Argon geochronology of small samples using the Vulkaan argon laserprobe, Proceedings of the Royal Netherlands Academy of Arts and Sciences, pp. 185-218.

96. Willett, S.D., Brandon, M.T., 2013. Some analytical methods for converting thermochronometric age to erosion rate. Geochemistry, Geophysics, Geosystems 14, 209-222.

97. Zanchi, A., Gaetani, M., 2011. The geology of the Karakoram range, Pakistan: the new 1: 100,000 geological map of Central-Western Karakoram. Italian journal of geosciences 130, 161-262.

98. Zanchi, A., Poli, S., Fumagalli, P., Gaetani, M., 2000. Mantle exhumation along the Tirich Mir Fault Zone, NW Pakistan: pre-mid-Cretaceous accretion of the Karakoram terrane to the Asian margin. Geological Society, London, Special Publications 170, 237-252.

99. Zeitler, P.K., Meltzer, A.S., Koons, P.O., Craw, D., Hallet, B., Chamberlain, C.P., Kidd, W.S., Park, S.K., Seeber, L., Bishop, M., 2001. Erosion, Himalayan geodynamics, and the geomorphology of metamorphism. GSA Today 11, 4-9.

100. Zeitler, P.K., 1985. Cooling history of the NW Himalaya, Pakistan. Tectonics 4, 127-151.

Click here to download Table Table 1.xlsx

Table 1. Sample collection site coordinates, draiange, and tectonic terranes.				
Sample	Drainage	Sourced terrane	Latitude	Longitude
MRS 3	Hunza River	Karakoram, Pamir	36.3119	74.6916
MRS 4	Gilgit	Karakoram, N Kohistan	35.9252	74.2656
MRS 2	Hunza, Danur, Gilgit	N Kohistan, Karakoram	35.8998	74.3968
MRS 5	Kesu, Chitral	Karakoram, Hindu Kush, Kohistan	35.6211	71.7967
MRS 8	Dir	Kohistan	35.1427	71.9018
MRS 9	Kabul, Hajizai	Swat Himalaya, Kohistan, Hindu Kush	34.1648	71.5927

Table 2. Summary of methods for the inversion of detrital thermochronometer ages to erosion rates.

Table 2. Summary of methods for the inversion of detrital thermochronometer ages to erosion rates

Inversion methods	**Method-1**	**Method-2**	**Method-3**	**Method-4**
Common assumptions	1. Vertical particle trajectory (no lateral variation)			
	2. Representative sampling (lithology control on detrital crystal yield)			
	3. Brief residence time in the sediment-transport system			
Characters of modeled erosion rate	Temporarily averaged (steady state)	Temporarily averaged (steady state)	Temporarily varying	Temporarily averaged (steady state)
	Basin-wide uniform	Basin-wide uniform	Basin-wide uniform	Spatially varying
Calculation of erosion rates	Using elevation-age relation			Erosion-dependence of timing of particle passage from closure isotherm to surface
	Mean elevation and age (point-point)	Range of elevations and ages	Piecewise (segment) elevation-age	
Drainage size	Small	Small	Large	Large
Suitable thermochronometers	$^{40}Ar/^{39}Ar$	$^{40}Ar/^{39}Ar$	Apatite U-Th/He & Apatite fission track (encouraged for $^{4}He/^{3}He$, $^{40}Ar/^{39}Ar$)	Apatite U-Th/He, apatite fission track, ziron U-Th/He, zircon fission track, $^{40}Ar/^{39}Ar$
Reference	Brewers et al., 2003; 2006	Hodges et al., 2005; Ruhl and Hodges, 2005	Duvall et al., 2012; Avdeev et al., 2011	Brandon et al., 1998; Garver and Brandon, 1999; Willett & Brandon, 2013

Figure 1

Click here to download Figure Figure1.jpg

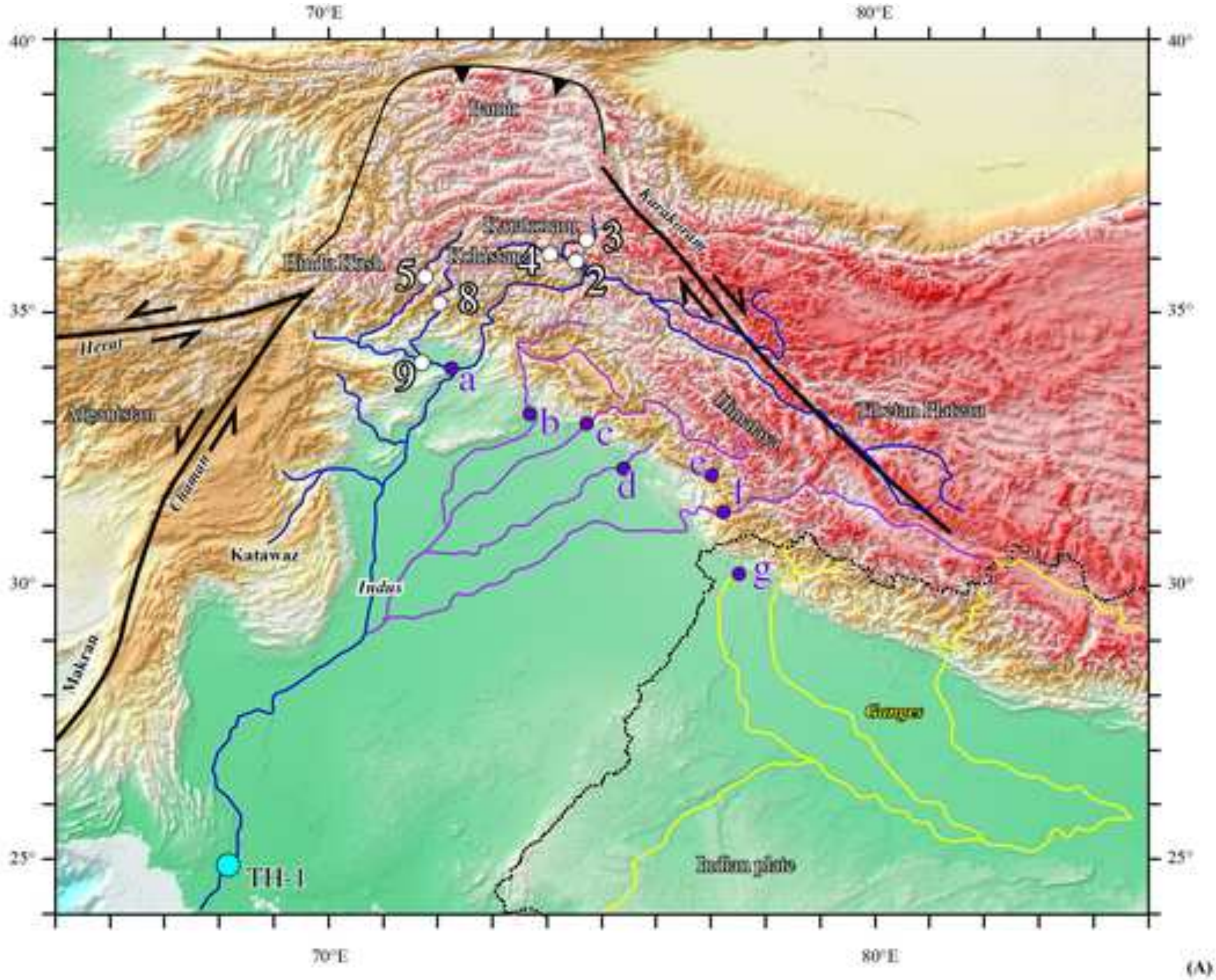

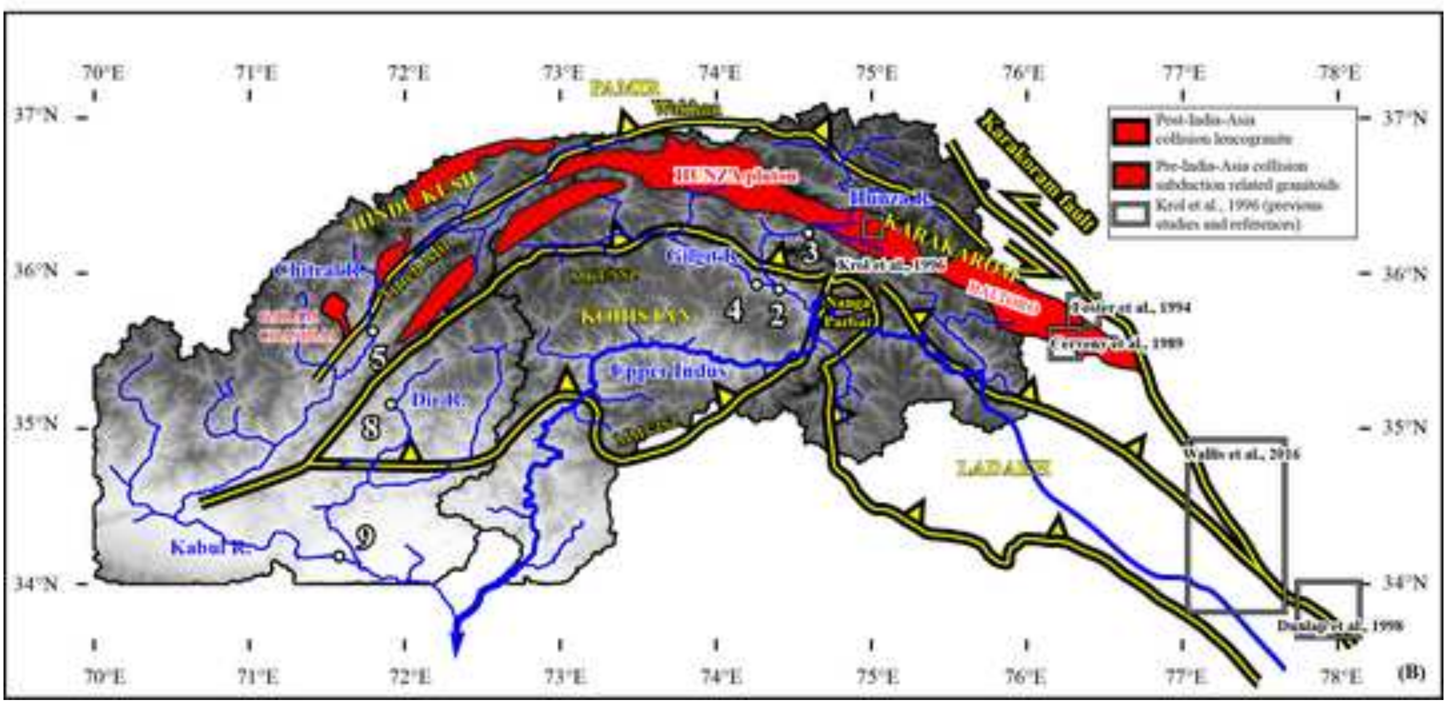

Figure 2

Click here to download Figure Figure2.jpg

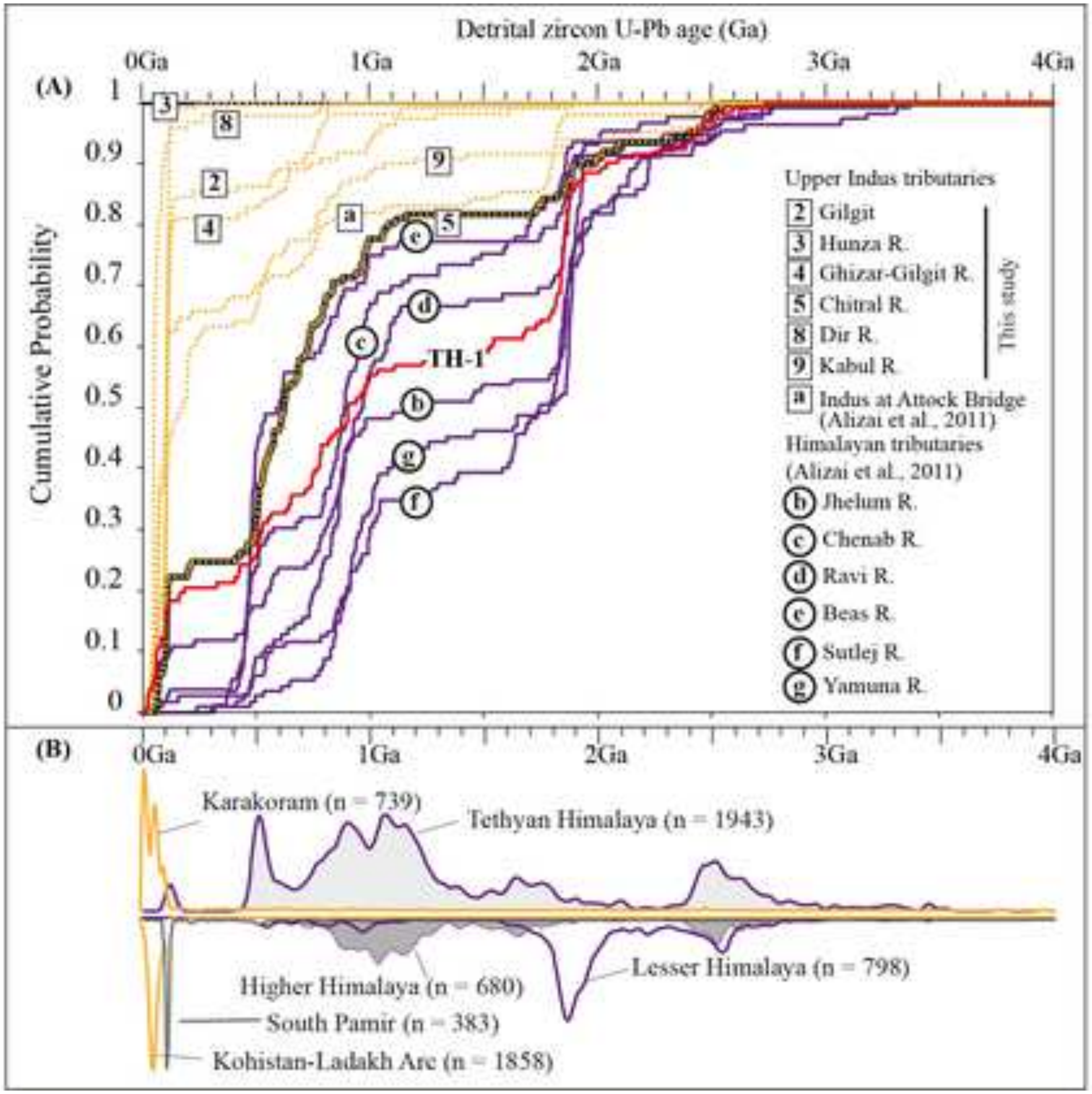

Figure 3

Click here to download Figure Figure3.jpg

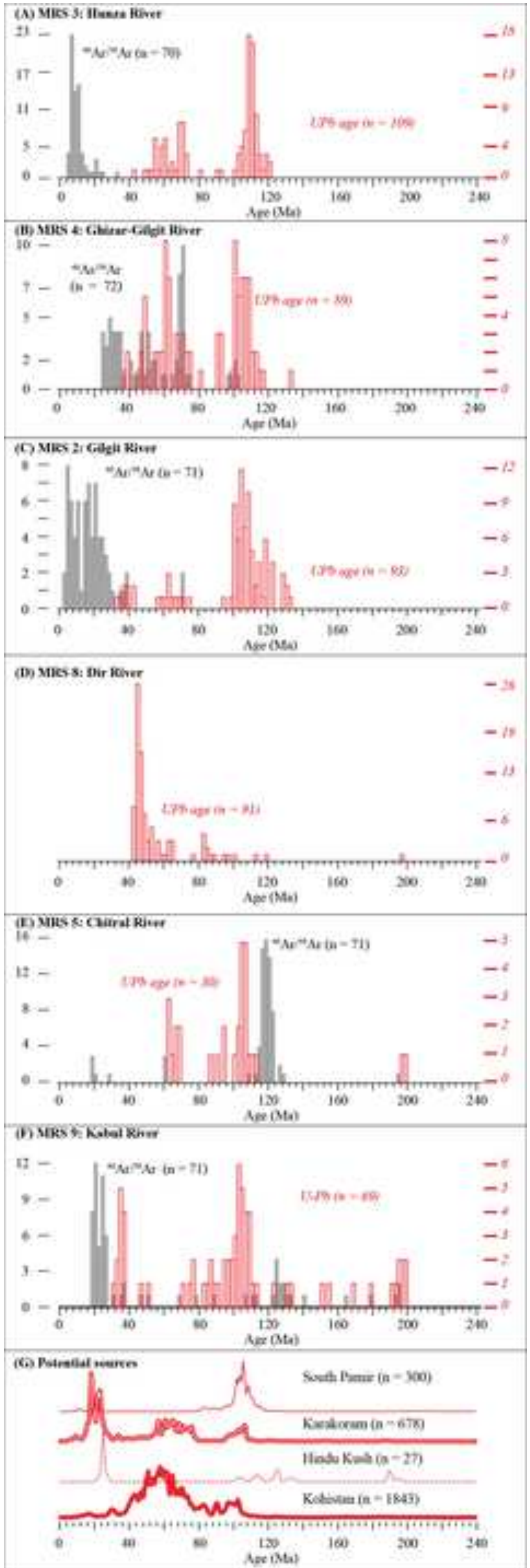

Figure 4

Click here to download Figure Figure4.jpg

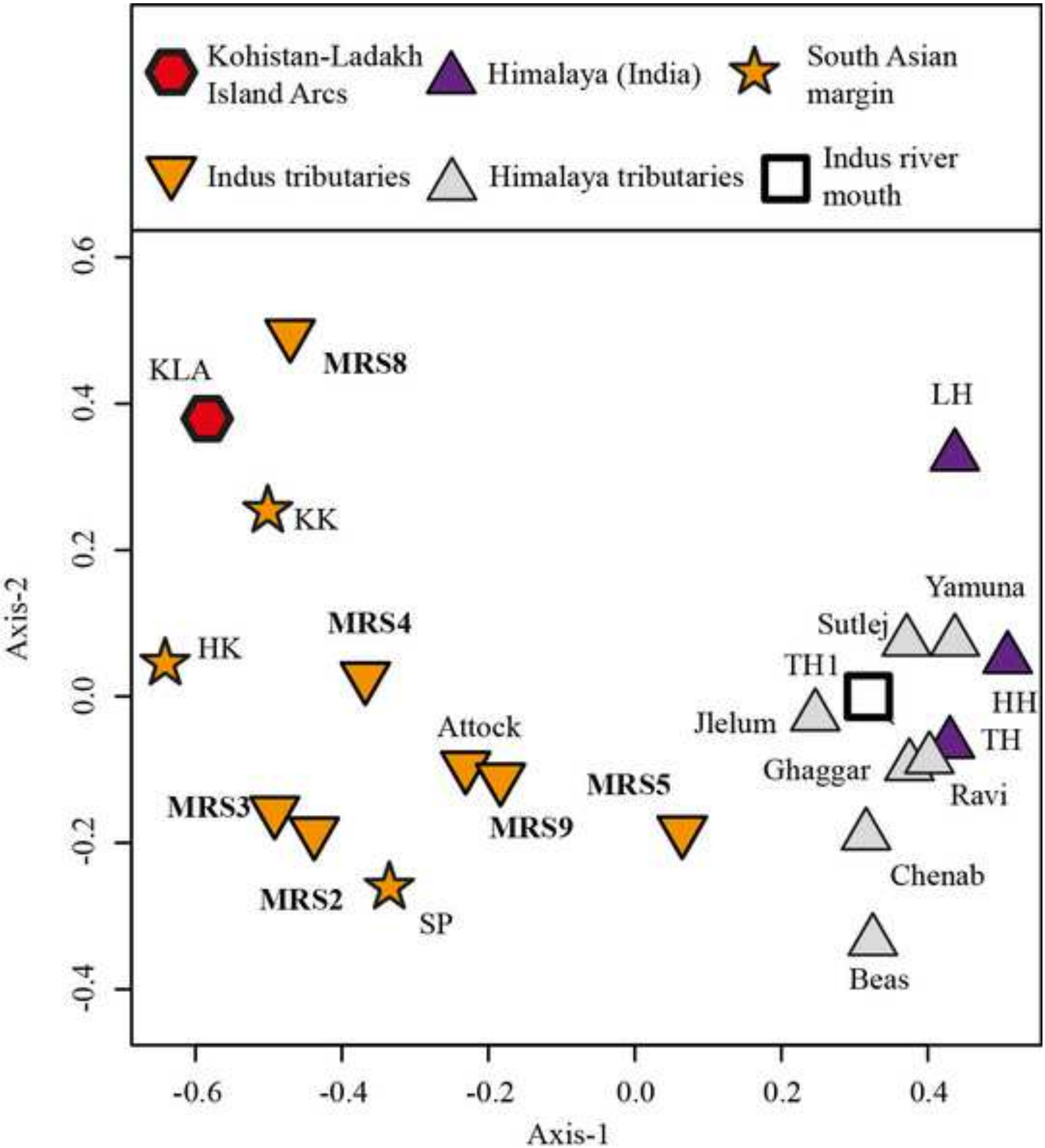

Figure 5

Click here to download Figure Figure5.jpg

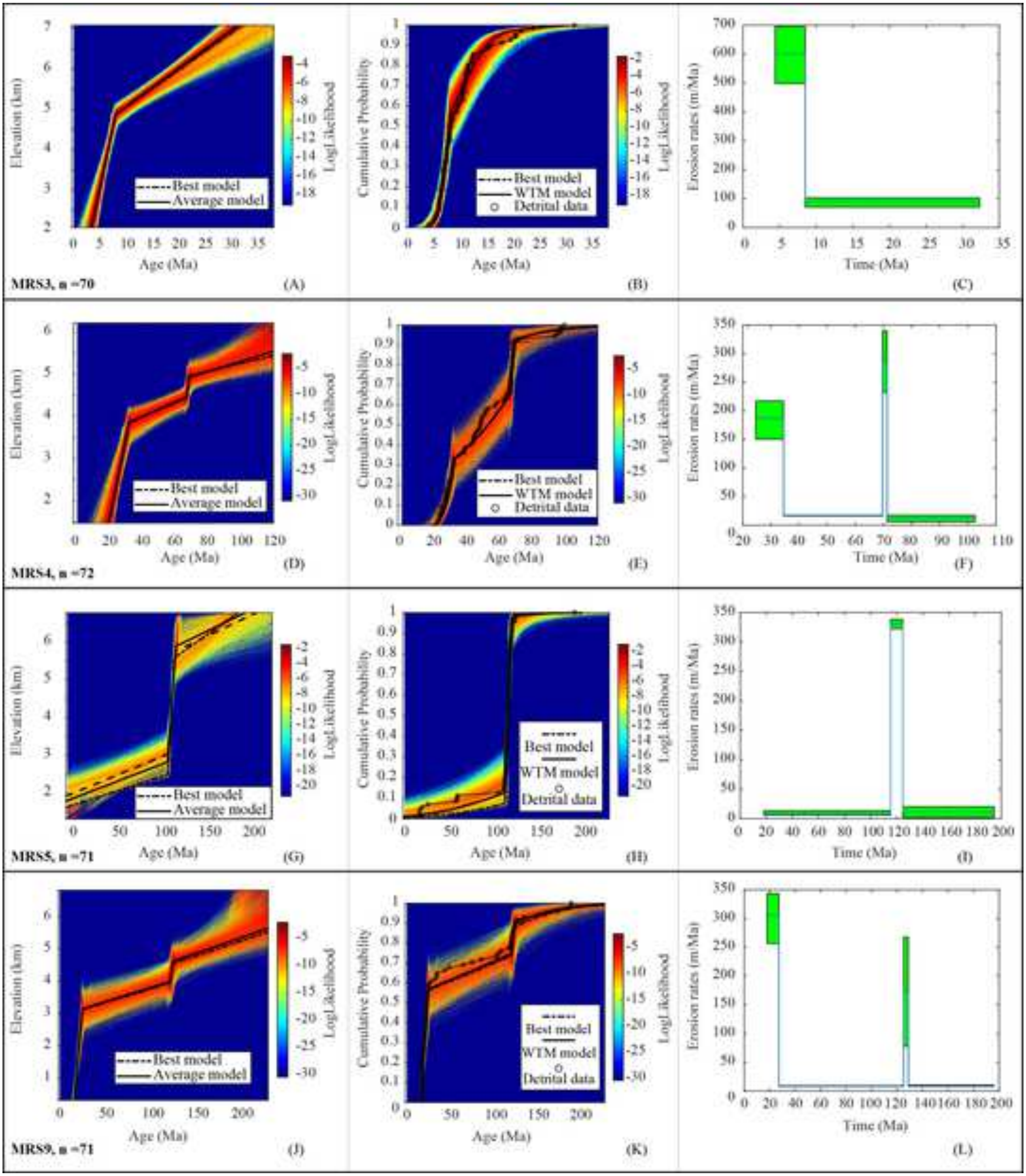

Figure 6

Click here to download Figure Figure6.jpg

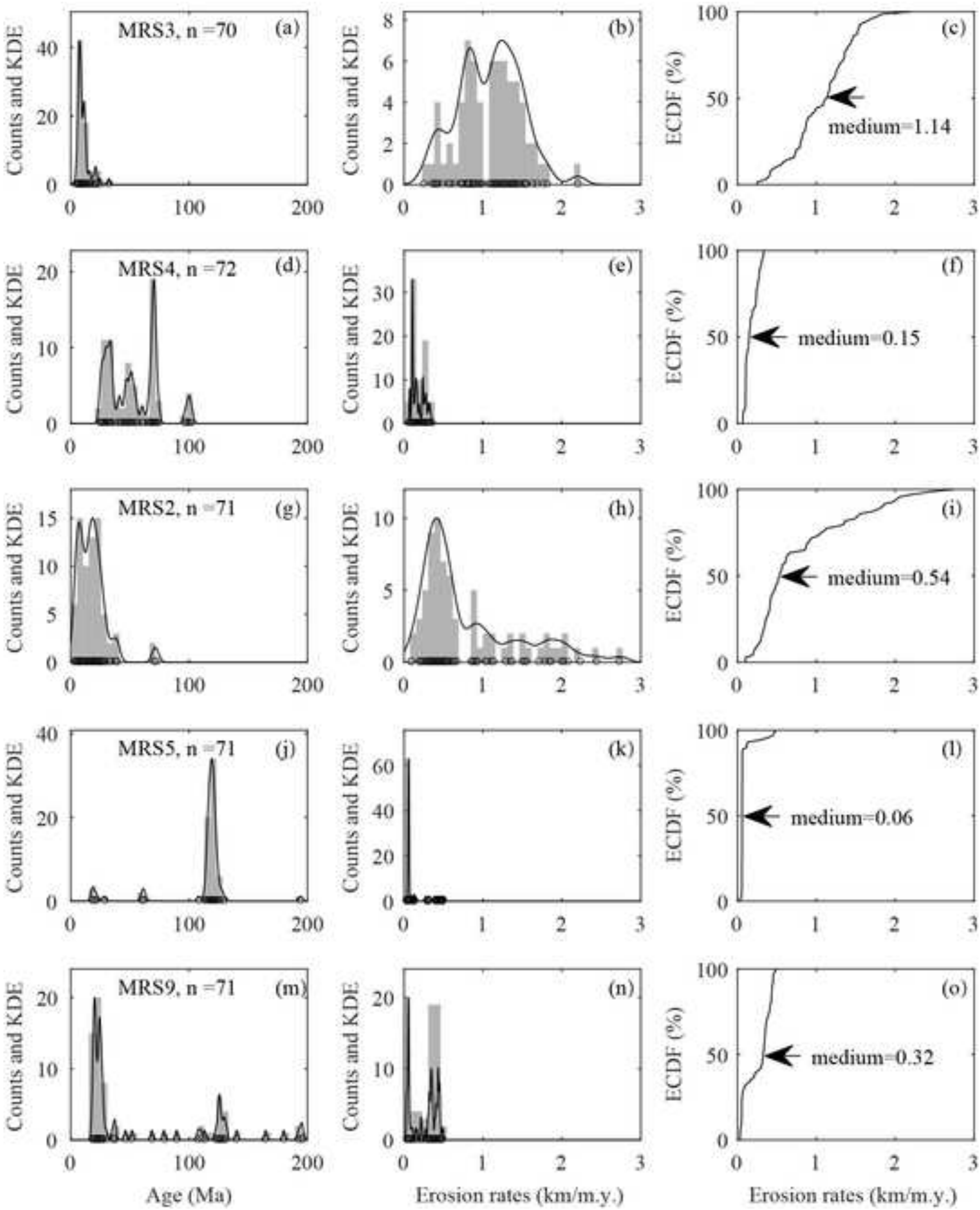

Table S1. Detrital zircon U-Pb ages.

Click here to access/download
Dataset
Table S1_UPb.xls

Table S2. Detrital muscovite single crytal 40Ar/39Ar ages.

Click here to access/download

Dataset

Table S2.xlsx

Table S3. Modeling results using Avdeev's method (Avdeev et al., 2011).

Click here to access/download
Dataset
Table S3_ModelingResults.xlsx